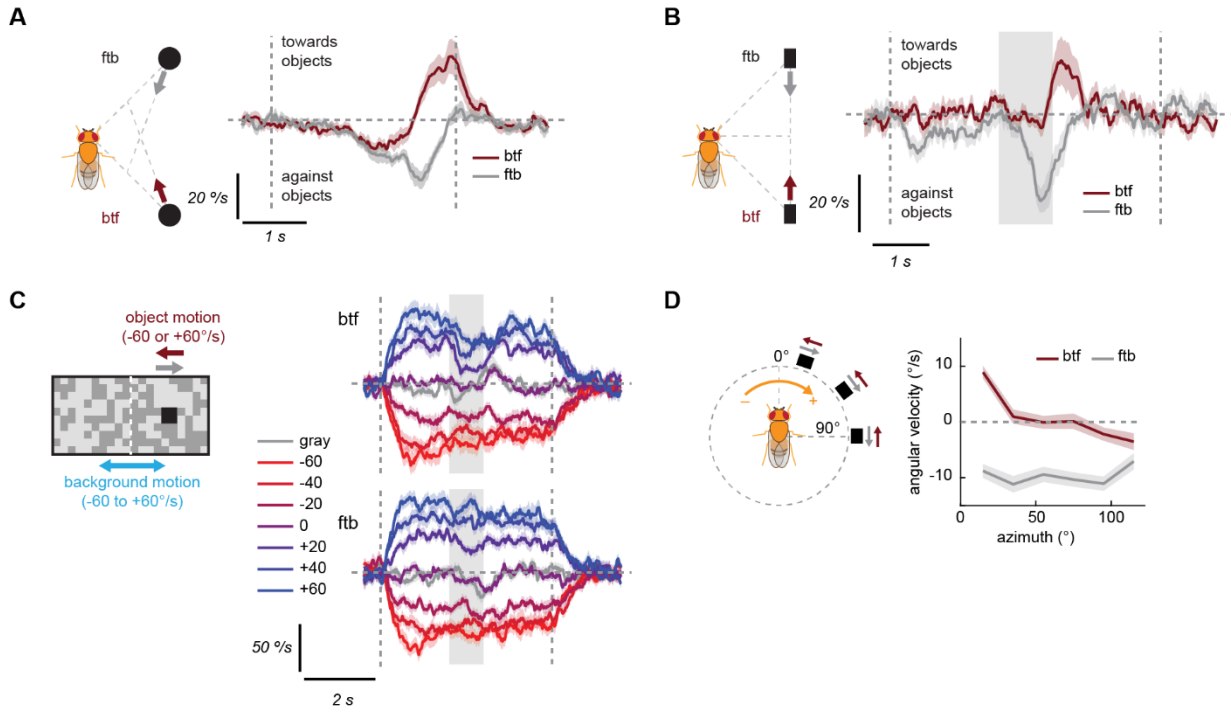

Figure S1. Fly turning responses to small object motion. Related to Figure 1.

(A) Turning responses of wildtype flies to the approach stimuli over time. Horizontal dotted lines mark zero turning. See also **Figure 1G**. (B) Turning responses of wildtype flies to the parallel stimuli over time. See also **Figure 1J**. (C) Turning responses of wildtype flies to squares paired with rotating backgrounds, by object directions and background velocities. See also **Figure 1M**. (D) Time-averaged turning responses of wildtype flies to horizontally moving squares, as functions of azimuthal positions of the squares. See also **Figure 1Q**. Across stimulus configurations, flies generally turned away from the front-to-back moving objects. They turned towards the side of the object primarily when it is in front of the fly and moving back-to-front. Error bars and shades around mean traces all indicate standard error of the mean. (A) N = 21 flies. (B) N = 19 flies. (C) N = 19 flies. (D) N = 39 flies.

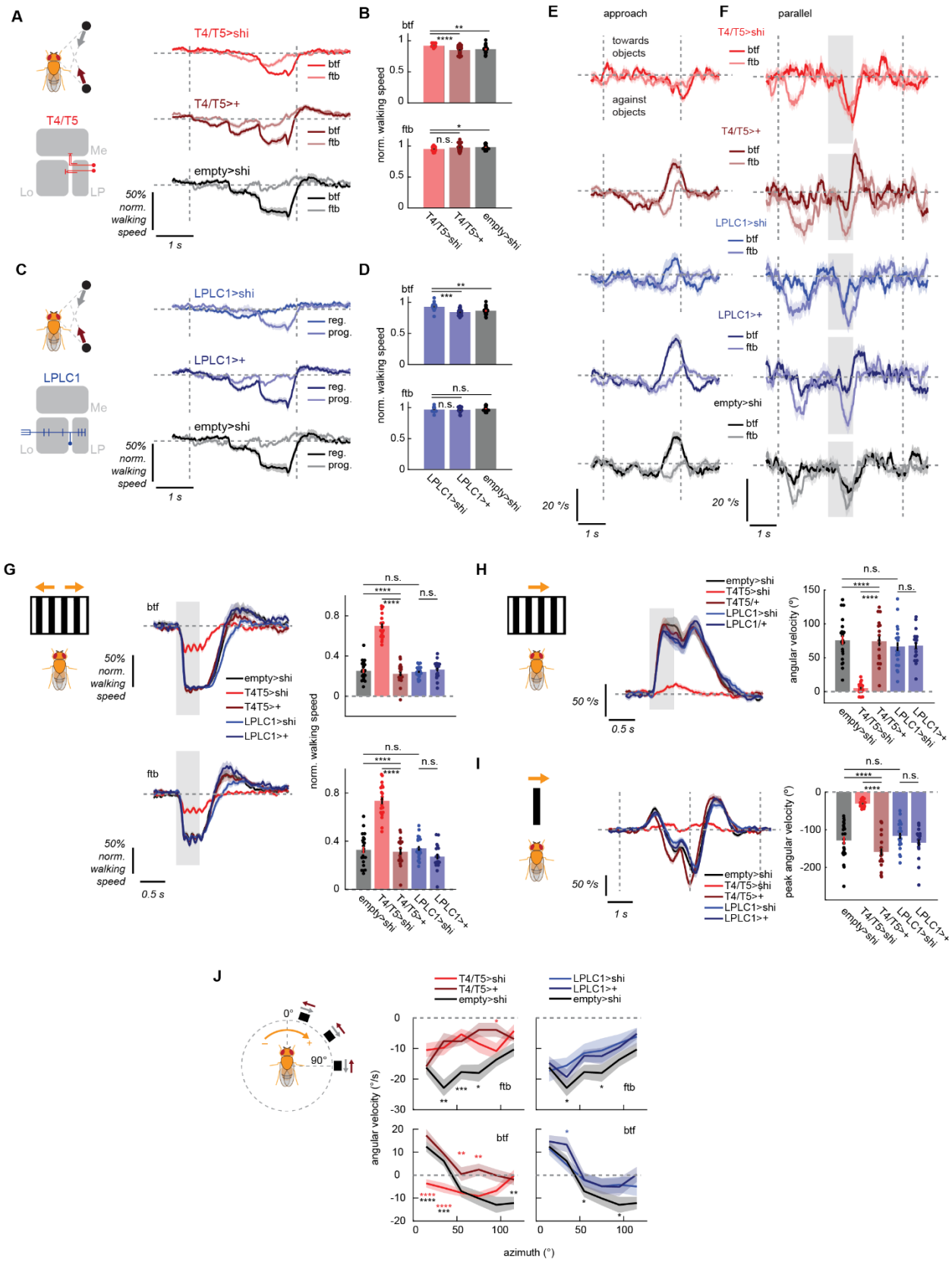
A
T4/T5
Me
Lo
LP
T4/T5>shi
T4/T5>+
empty>shi
btf
ftb
50% norm. walking speed
1 s
B
norm. walking speed
n.s.
T4/T5>shi
T4/T5>+
empty>shi
C
LPLC1
LPLC1>shi
LPLC1>+
reg.
prog.
D
E
approach
towards objects
against objects
20 °/s
F
parallel
G
0.5 s
H
empty>shi
T4T5>shi
T4T5/+
LPLC1>shi
LPLC1/+
angular velocity (°)
50 °/s
I
peak angular velocity (°)
J
0°
90°
T4/T5>shi
T4/T5>+
empty>shi
LPLC1>shi
LPLC1>+
angular velocity (°/s)
azimuth (°)

Figure S2. Additional behavioral effects of silencing T4/T5 and LPLC1. Related to Figure 2.

(A-D) Normalized walking responses of flies to the approach stimuli with (A, B) T4/T5 or (C, D) LPLC1 silenced and their respective genetic controls, either (A, C) over time or (B, D) time-averaged, as in **Figure 1G, H**. While silencing T4/T5 and LPLC1 both significantly reduced slowing, apparent directional biases in the behavior remained after silencing. This is presumably due to preferential slowing in response to looming in front rather than behind, implemented by T4/T5 independent, loom-sensitive neurons, such as LC4[S1], LC6 [S2], or LC16 [S3]. (E, F) Turning responses of flies with T4/T5 or LPLC1 silencing and their corresponding genetic controls, in response to the (E) approach or (F) parallel stimuli, as in **Figure S1A, B**. (G-I) Examples of T4/T5-dependent behaviors where LPLC1 is dispensable. (G) Slowing responses of flies with T4/T5 or LPLC1 silencing and their controls to translational gratings either back-to-front or front-to-back, either (*left*) over time or (*right*) time-averaged. (H) Optomotor turning responses of flies with T4/T5 or LPLC1 silencing and their controls to drifting gratings, either (*left*) over time or (*right*) time-averaged. (I) Aversive turning responses of flies with T4/T5 or LPLC1 silencing and their controls to fast translating vertical bars, either (*left*) over time or (*right*) peak turning amplitudes. The gratings had a period of 60º and temporal frequency of 8 Hz. The bar was 10º wide and moved at 60 º/s. (J) Turning responses of flies with T4/T5 or LPLC1 silencing and their corresponding genetic controls, in response to horizontally moving squares at different azimuthal positions, as in **Figure S1D**. Silencing of T4/T5 abolished flies turning towards the frontal objects moving back-to-front, revealing position-aversive component of the turning. Error bars and shades around mean traces all indicate standard error of the mean. (A-E) N = 20 (T4/T5>shi), 23 (T4T5>+), N = 16 (LPLC1>shi), 21 (LPLC1>+), 21 (empty>shi) flies. (F, G-I) N = 19 (T4/T5>shi), 17 (T4/T5>+), N = 20 (LPLC1 >shi), 17 (LPLC1>+), 22 (empty>shi) flies. (J) N = 18 (T4/T5>shi), 20 (T4/T5>+), 19 (LPLC1>shi), 16 (LPLC1>+), 19 (empty>shi) flies. n. s.: not significant ($p > .05$); *: $p < .05$; **: $p < .01$; ***: $p < .001$; ****: $p < .0001$ in Wilcoxon rank sum test. Colored and black stars indicate the comparisons between the experimental and Gal4-only or UAS-only controls, respectively.

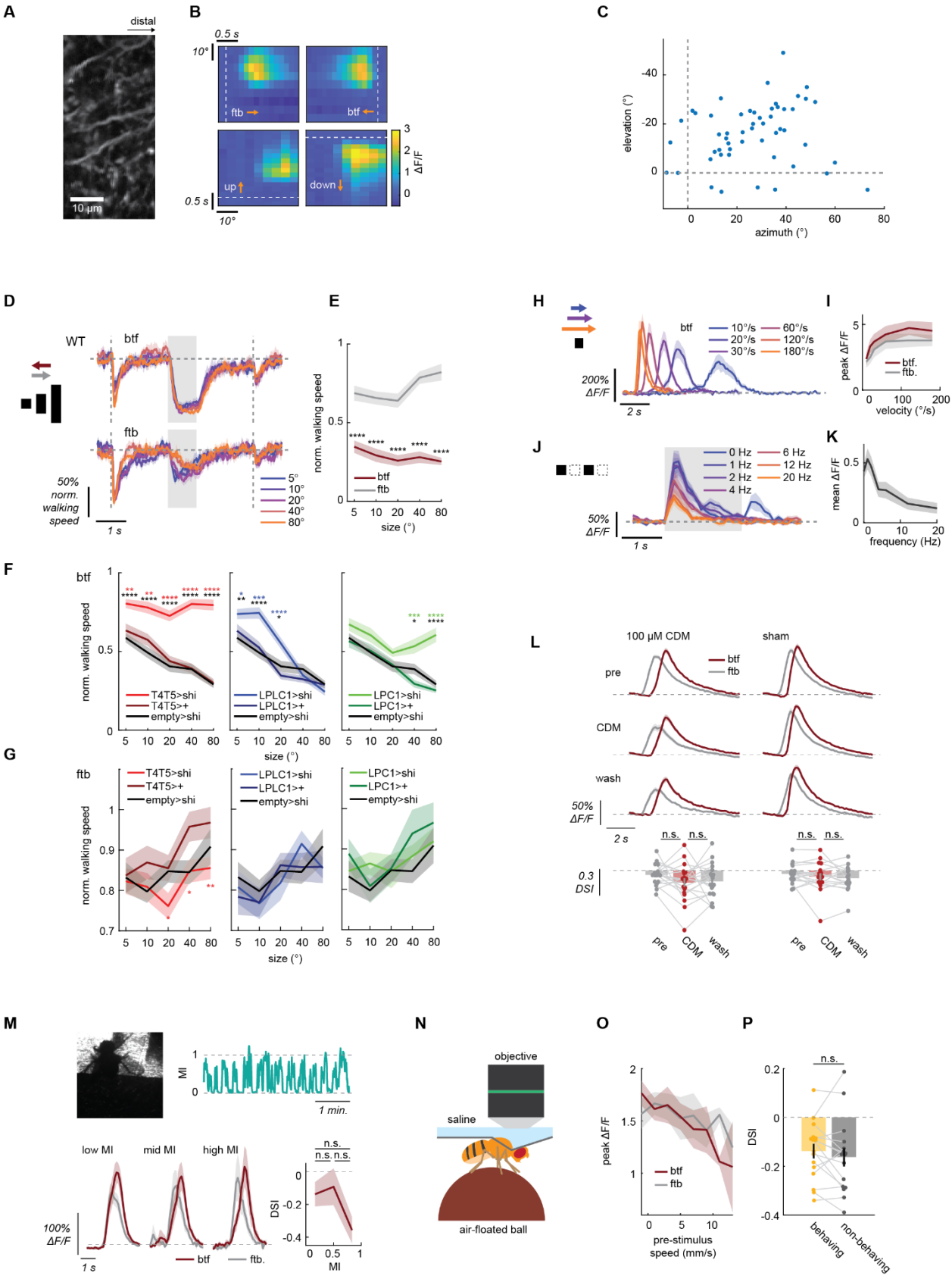
A
distal
10 µm
B
0.5 s
10°
ftb
btf
up
down
0.5 s
10°
3
2
1
0
ΔF/F
C
elevation (°)
azimuth (°)
D
WT
btf
ftb
50% norm. walking speed
1 s
5°
10°
20°
40°
80°
E
norm. walking speed
btf
ftb
size (°)
H
btf
10°/s
20°/s
30°/s
60°/s
120°/s
180°/s
200% ΔF/F
2 s
I
peak ΔF/F
btf.
ftb.
velocity (°/s)
J
0 Hz
1 Hz
2 Hz
4 Hz
6 Hz
12 Hz
20 Hz
50% ΔF/F
1 s
K
mean ΔF/F
frequency (Hz)
F
btf
norm. walking speed
T4T5>shi
T4T5>+
empty>shi
LPLC1>shi
LPLC1>+
empty>shi
LPC1>shi
LPC1>+
empty>shi
size (°)
G
ftb
norm. walking speed
size (°)
L
100 µM CDM
sham
pre
CDM
wash
btf
ftb
50% ΔF/F
2 s
n.s.
0.3 DSI
pre
CDM
wash
M
MI
1 min.
low MI
mid MI
high MI
100% ΔF/F
1 s
btf
ftb.
DSI
MI
N
objective
saline
air-floated ball
O
peak ΔF/F
btf
ftb
pre-stimulus speed (mm/s)
P
DSI
n.s.
behaving
non-behaving

Figure S3. Additional characterizations of LPLC1 cell response properties and their behavioral consequences. Related to Figure 3.

(A) A representative time-averaged image of LPLC1 lobula neurites during single cell recordings. (B) Responses of an example cell to receptive field mapping stimuli (a 10° x 10° translating black square). The square swept a 40° x 40° area around the approximated RF center in the four directions with the resolution of 5°. (C) Distribution of estimated RF locations of individual LPLC1 lobula neurites. Only cells with good Gaussian fits on the both horizontal and vertical dimensions are plotted. (D, E) Wildtype fly slowing response to horizontally translating objects with different heights in either direction, either (D) over time or (E) as functions of the heights. Flies slow more in response to objects moving back-to-front across the all sizes tested. (F) Slowing responses of flies with (*left*) T4/T5, (*middle*) LPLC1, or (*right*) LPC1 silenced and their respective controls to objects with various heights, moving back-to-front. While silencing of T4/T5 reduces slowing across the all sizes tested, LPLC1 and LPC1 silencing only affects slowing caused by short and tall objects, respectively, revealing complementary contributions to behavior of these two visual projection neurons. (G) The same as (F), but for objects moving front-to-back, where these manipulations had little effect. (H-K) Calcium responses of LPLC1 neurons to small squares either (H, I) translating at various velocities or (J, K) flickering on the spot at various temporal frequencies, either over time or as functions of the velocity/temporal frequency. (L-P) Additional experiments to show that behavioral states of the flies as (L) manipulated by chlordimeform (CDM) application or as quantified by (M) leg movements and (N-P) forward walking speed do not correlate with the physiologically measured direction selectivity of LPLC1 neurons. (L) (*top*) Calcium responses of LPLC1 neurons in response to horizontally translating objects over time and (*bottom*) their direction selectivity index (DSI), before, during, and after 100 μM CDM application. The "sham" control flies (*right*) were included to exclude the possibility that potential effects of CDM application simply reflected the effect of the passage of time. While CDM has been shown to modulate response properties of some lobula columnar VPN types in *Drosophila* [S4], it did not affect the direction selectivity of LPLC1. (M) (*top left*) A typical image of a fly during an imaging experiment, taken from below. (*top right*) A typical time trace of movement index (MI), which represents normalized pixel intensity changes caused by the fly's leg movements [S5]. (*bottom left*) Fly-averaged calcium responses of LPLC1 to translating black rectangular objects, sorted by the mean MI during the two seconds preceding the stimulus onset. (*bottom right*) DSI of LPLC1 calcium responses to translating black objects, as a function of pre-stimulus mean MI. The leg movements of the flies did not correlate with the direction selectivity of LPLC1. (N) A schematic of the simultaneous behavioral and physiological recording setup. An air-floated ball with a position-reader identical to **Figure 1E** was inserted under the setup shown in **Figure 3A**. The holder was designed to provide enough clearance for the thorax and abdomen such that flies can walk [S6]. The panoramic screen on which stimuli were presented is omitted from the schematic. (O) Fly-averaged peak calcium responses of LPLC1 to objects moving either way, as functions of mean absolute walking speed during the 1 second preceding the stimulus onset. (P) DSI of calcium responses of LPLC1 to moving objects, calculated separately for behaving trials (defined as mean pre-stimulus walking speed of more than 0.5 mm/s) and non-behaving trials. Each dot represents a single fly, and data from the same fly are connected by gray lines. Error bars and shading around mean traces all indicate standard error of the mean across (D-G, N-P) flies or (H-K) cells. (C) N =

53 cells. (D, E) N = 16 flies. (F, G) N = 21 (T4/T5>shi), 18 (T4/T5>+), 19 (LPLC1>shi), 18 (LPLC1>+), 20 (LPC1>shi), 19 (LPC1>+), 21 (empty>shi) flies. (H, I) N = 11 cells. (J, K) N = 12 cells. (L) N = 19 (CDM), 18 (sham). (M) N = 12. (O) N = 18. (P) N = 16 (2 flies in O did not have enough behaving trials to calculate DSI). n. s.: not significant ($p > .05$); *: $p < .05$; **: $p < .01$; ***: $p < .001$; ****: $p < .0001$ in Wilcoxon signed-rank (E, L, M, P) or rank sum test (F, G).

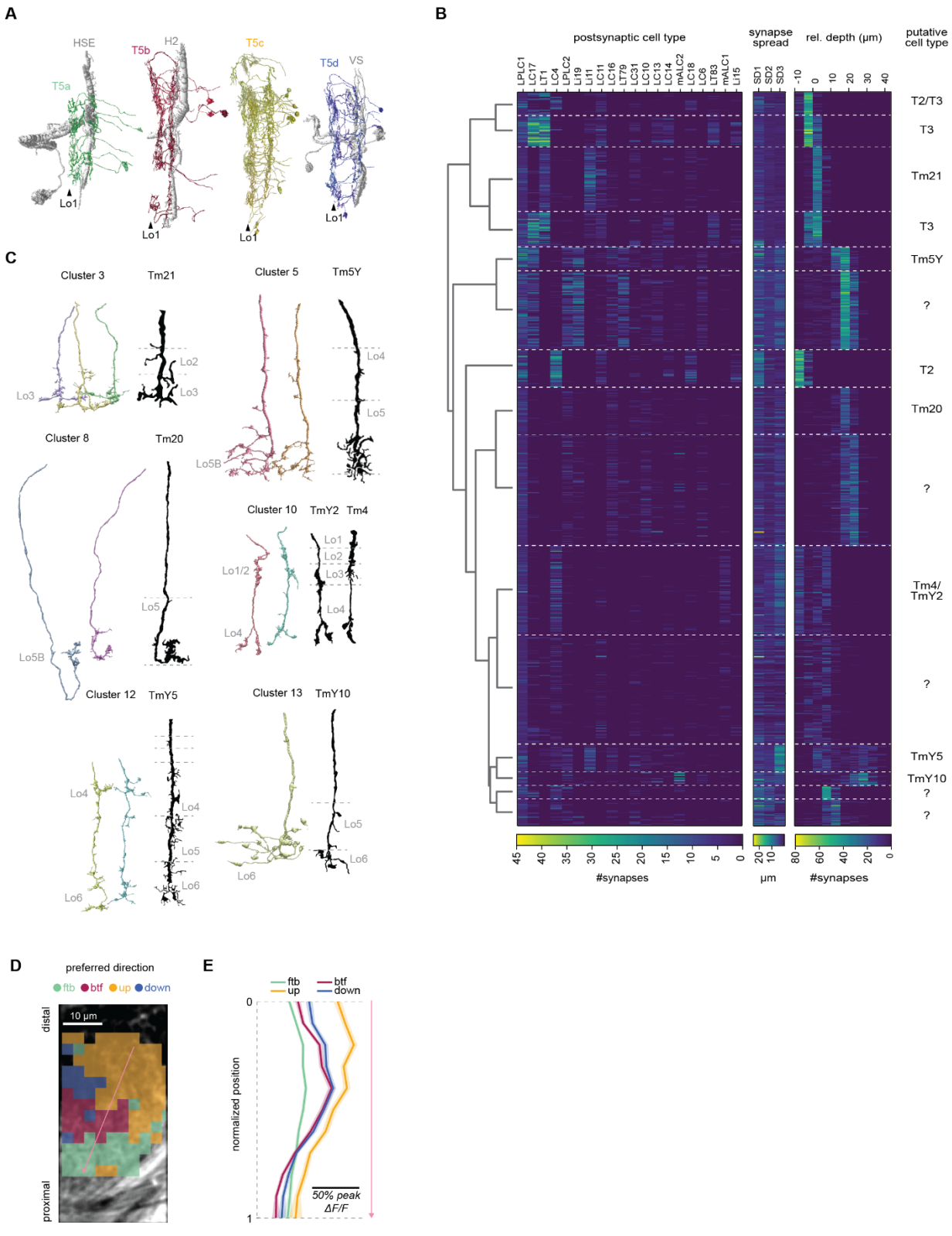
A
HSE
T5a
T5b
H2
T5c
T5d
VS
Lo1
B
postsynaptic cell type
synapse spread
rel. depth (µm)
putative cell type
LPLC1
LC17
LT1
LC4
LPLC2
LI19
LI11
LC11
LC16
LT79
LC31
LC10
LC13
LC14
mALC2
LC18
LC6
LT83
mALC1
LI15
SD1
SD2
SD3
T2/T3
T3
Tm21
T3
Tm5Y
?
T2
Tm20
?
Tm4/ TmY2
?
TmY5
TmY10
?
?
#synapses
µm
#synapses
C
Cluster 3
Tm21
Cluster 5
Tm5Y
Lo2
Lo3
Lo4
Lo5
Lo5B
Cluster 8
Tm20
Cluster 10
TmY2
Tm4
Lo1
Lo2
Lo3
Lo4
Lo1/2
Cluster 12
TmY5
Cluster 13
TmY10
Lo6
D
preferred direction
ftb
btf
up
down
10 µm
distal
proximal
E
normalized position
50% peak ΔF/F

Figure S4. Additional characterization of LPLC1 inputs. Related to Figure 4.

(A) Example T5 cells grouped by their subtypes, with their postsynaptic tangential neurons. (B) Three feature matrices used for lobula terminal clustering, representing (*left*) connectivity to downstream cell types, (*middle*) spatial spread of synapses along the three axes, and (*right*) innervation depth relative to LT1 are shown. Each row corresponds to a single terminal fragment. The dendrogram on the left shows the result of the agglomerative clustering. The putative cell type labels are shown on the right. Only the top 20 postsynaptic cell types are visualized. See also **Data S1**. (C) Reconstructed single-cell morphology of example neurons from clusters that resembled known cell types, alongside previously published Golgi-staining (in black) [S7]. (D) An example image of lobula plate expressing iGluSnFR panneuronally (nSyb > iGluSnFR), in which ROIs are color coded according to the direction of the bar to which they responded best, similar to **Figure 4J**. (E) Peak glutamatergic signals in lobula plate, as functions of normalized positions of ROIs along the layers of lobula plate, measured from the distal most layer. Similar to **Figure 4K**. Glutamate signals in the near layer 1 (normalized position 1) responded more to front-to-back than back to front, while closer to layer 2, the back-to-front signals are larger, suggesting intra-layer glutamate signaling. N = 17 (flies), 1595 (ROIs).

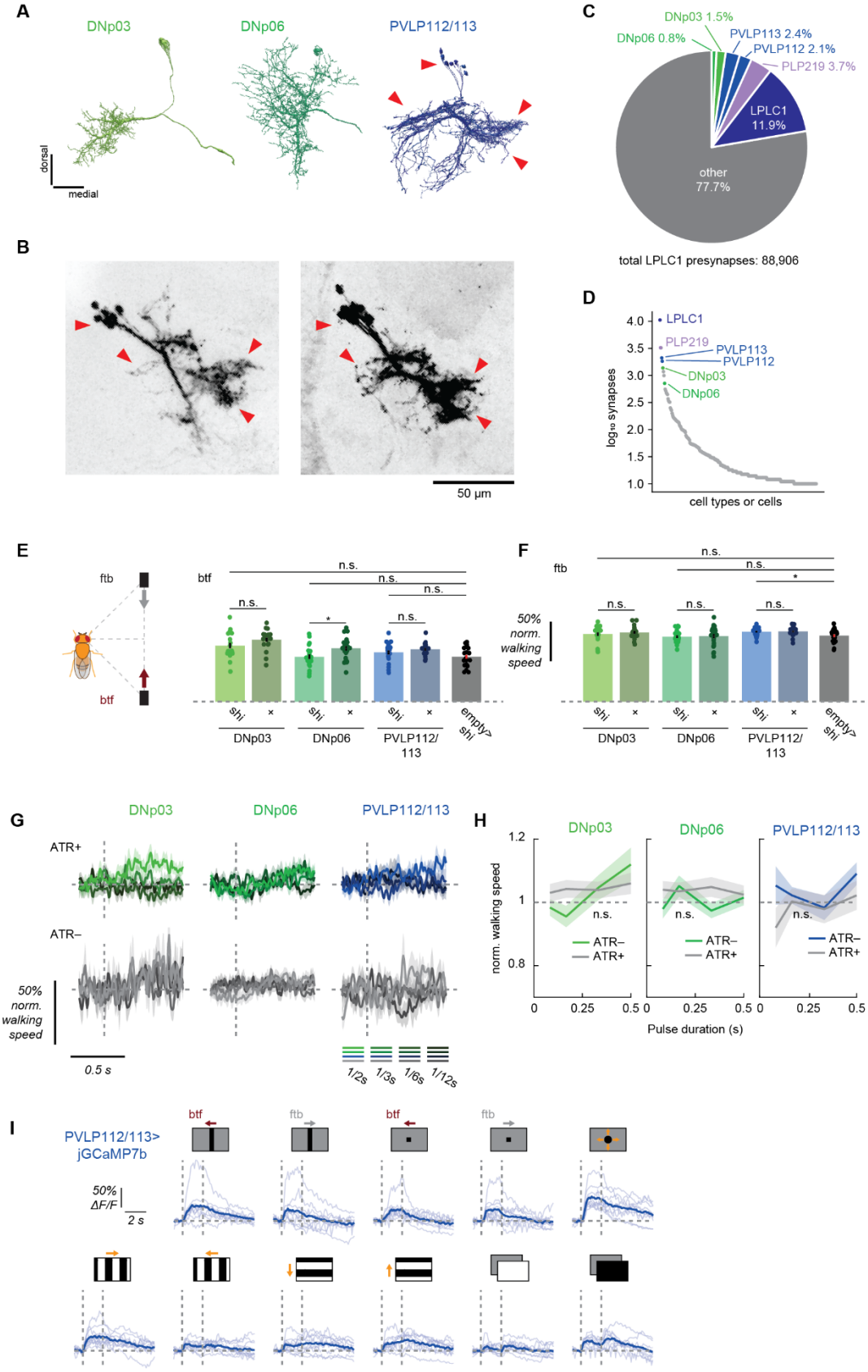
A
DNp03
DNp06
PVLP112/113
dorsal
medial
C
DNp03 1.5%
DNp06 0.8%
PVLP113 2.4%
PVLP112 2.1%
PLP219 3.7%
LPLC1 11.9%
other 77.7%
total LPLC1 presynapses: 88,906
B
50 µm
D
LPLC1
PLP219
PVLP113
PVLP112
DNp03
DNp06
log10 synapses
cell types or cells
E
ftb
btf
n.s.
*
shi
×
empty> shi
DNp03
DNp06
PVLP112/ 113
F
50% norm. walking speed
G
DNp03
DNp06
PVLP112/113
ATR+
ATR–
50% norm. walking speed
0.5 s
1/2s
1/3s
1/6s
1/12s
H
norm. walking speed
ATR–
ATR+
Pulse duration (s)
I
PVLP112/113> jGCaMP7b
50% ΔF/F
2 s

Figure S5. Neurons downstream of LPLC1. Related to Figure 5.

(A) Reconstructed morphology of DNp03, DNp06, and PLP112/113 from the hemibrain dataset[S8]. (B) PVLP112/113 neurons visualized with UAS-myr::GFP using newly generated split Gal4 lines. (*left*) R72A10AD; VT002042DBD (*right*) R72A10AD; VT019749DBD. Corresponding structures between (A) and (B) are marked with the red arrows. The first driver was used for the behavioral experiments. See also **Videos S3, 4** for the expression pattern across the entire brain. (C) Counts of LPLC1 output synapses by postsynaptic cell types. (D) Distribution of synaptic weights from LPLC1 to downstream neurons. Downstream neurons are grouped into cell types if they are labeled, and separately counted as individual neurons if not. While the downstream cell types studied here only account for up to several percent of total LPLC1 outputs individually, the distribution of connections is heavily skewed and most other cell types had many fewer synapses. Cells with less than 10 total synapses from LPLC1 are not visualized. (E, F) Time-averaged normalized walking responses of flies to the parallel stimulus in (E) back-to-front and (F) front-to-back directions, with noted downstream neuron silenced and corresponding controls. (G, H) Normalized walking responses of flies expressing Chrimson in PVLP112/113, DNp03, or DNp06 to pulses of green lights, visualized (G) over time or (H) averaged over time. (I) Individual (light blue) and fly-averaged (dark blue) calcium responses of PVLP112/113 population over time to a variety of visual stimuli (horizontally moving bars and squares, looming, square wave gratings, full-field flashes). Leftward in the stimulus schematics corresponds to the back-to-front direction. Error bars and shades around mean traces all indicate standard error of the mean. (E, F) N = 17 (DNp03>shi), 19 (DNp03>+), 19 (DNp06>shi), 24 (DNp06>+), 19 (PVLP112/113>shi), 17 (PVLP112/113>+), 22 (empty>shi). (G, H) N = 14 (DNp03, ATR+), 13 (DNp03, ATR-), 13 (DNp06, ATR+), 15 (DNp03, ATR-), 12 (PVLP112/113, ATR+), 6 (PVLP112/113, ATR-). (I) N = 10. n. s.: not significant ($p > .05$); *: $p < .05$; **: $p < .01$; ***: $p < .001$; ****: $p < .0001$ in Wilcoxon rank sum test (E, F) and 2-way analysis of variance (ANOVA) (H; the main effect of ATR conditions).

Description	Genotype	Figure
wildtype	+; +; +	1, S1, S3DE
empty>shi	w/+; AD/UAS-shi^{ts}; DBD/UAS-shi^{ts}	2A-F, 5CD, S2, S3FG, S5EF
T4T5>shi	w/+; R59E08AD/UAS-shi^{ts}; R42F06DBD/UAS-shi^{ts}	2ABEF, S2ABEFG-J, S3FG
T4T5>+	w/+; R59E08AD/+; R42F06DBD/+	2ABEF, S2ABEFG-J, S3FG
LPLC1>shi	w/+; R64G09AD/UAS-shi^{ts}; R37H04DBD/UAS-shi^{ts}	2CDEF, S2CDEFG-J, S3FG
LPLC1>+	w/+; R64G09AD/+; R37H04DBD/+	2CDEF, S2CDEFG-J, S3FG
LPC1>shi	w/+; R81A05AD/UAS-shi^{ts}; T031495DBD/UAS-shi^{ts}	S3FG
LPC1>+	w/+; R81A05AD /+; VT031495DBD /+	S3FG
norpA^{-}; LPLC1>Chrimson	norpA^{7}; R64G09AD/+; R37H04DBD/UAS-CsChrimson.mVenus	2HI
LPLC1>GCaMP6f	+; UAS-GCaMP6f; R36B06Gal4	3B-M, S3A-CH-KM
LPLC1>jGCaMP7b	+; +; R36B06Gal4 UAS-jGCaMP7b	3NO, S3LN-P
LPLC1>jGCaMP7b; T4/T5>Chrimson	w/+; R42F06lexA/+; R36B06Gal4 UAS-jGCaMP7b/LexAop-CsChrimson.tdTomato	4CD
LPLC1>iGluSnFR	w/+; R64G09AD/UAS-iGluSnFR; R37H04DBD/UAS-iGluSnFR+	4H-KQR
nSyb>iGluSnFR	+; +; nSyb-Gal4/UAS-iGluSnFR	S4DE
LPLC1>GCaMP6f, GluClαRNAi, Dicer2	y, v/+; UAS-GCaMP6f/UAS-GluClαRNAi; R36B06Gal4/UAS-Dicer2	4L-N
LPLC1>GCaMP6f, Dicer2	+; UAS-GCaMP6f/UAS-Dicer2; R36B06Gal4/+	4L-N
LPLC1>jGCaMP7b, GluClαRNAi, Dicer2	y, v/+; UAS-GluClαRNAi/+; R36B06Gal4, UAS-jGCaMP7b/UAS-Dicer2	4OP
LPLC1>jGCaMP7b, Dicer2	+; UAS-Dicer2/+; R36B06Gal4, UAS-jGCaMP7b/+	4OP
PVLP112/113>GFP (A)	w/+; R72A10AD/+; VT002042DBD/UAS-myr::GFP	S4B
PVLP112/113>GFP (B)	w/+; R72A10AD/+; VT019749DBD/UAS-myr::GFP	S4B

PLP219>GFP	w/+; VT041832AD/+; VT021792DBD/UAS-myr::GFP	5B
DNp03>shi	w/+; R91C05AD/UAS-shi^{ts}; R31B08DBD/ UAS-shi^{ts}	S4DE
DNp03>+	w/+; R91C05AD/+; R31B08DBD/+	S4EF
DNp06>shi	w/+; VT019018AD/UAS-shi^{ts}; VT017411/UAS-shi^{ts}	S4EF
DNp06>+	w/+; VT019018AD/+; VT017411/+	S4EF
PVLP112/113>shi	+; R72A10/UAS-shi^{ts}; VT002042DBD/UAS-shi^{ts}	S4EF
PVLP112/113>+	+; R72A10/+; VT002042DBD/+	S4EF
PLP219>shi	+; VT041832/UAS-shi^{ts}; VT021792/UAS-shi^{ts}	5CD
PLP219>+	+; VT041832/+; VT021792/+	5CD
norpA^{-}; DNp03>Chrimson	norpA^{7}; R91C05AD/+; R31B08/UAS-CsChrimson.mVenus	S4GH
norpA^{-}; DNp06>Chrimson	norpA^{7}; VT019018AD/+; VT017411/UAS-CsChrimson.mVenus	S4GH
norpA^{-}; PVLP112/113>Chrimson	norpA^{7}; R72A10AD/+; VT002042DBD/UAS-CsChrimson.mVenus	S4GH
norpA^{-}; PLP219>Chrimson	norpA^{7}; VT-41832AD/+; VT021792/UAS-CsChrimson.mVenus	5EF
PLP219>jGCaMP7b	w/+; VT041832AD/+; VT021792DBD/UAS-jGCaMP7b	5G
PVLP112/113>jGCaMP7b	w/+; R72A10AD/+; VT002042DBD/UAS-jGCaMP7b	S4I
PVLP112/113>jGCaMP7b	w/+; R72A10AD/+; VT019749DBD/UAS-jGCaMP7b	S4I

Table S1. Genotypes of flies used in the experiments. Related to STAR Methods.

Behavioral experiments		
Stimulus	Description (duration)	Figures
Approach stimulus	A cylindrical column with 3 mm diameter and 2 mm height appeared 30 mm to the side and 30 mm ahead or behind the fly, then approached the fly with the velocity of 15 mm/s along the axis parallel to the fly's heading and 7.5 mm/s along the perpendicular axis. (2.67 s)	1F-H, S1A, S2A-E
Parallel stimulus	A 3 mm wide and 2 mm tall rectangular object appeared 15 mm to the side and 15 mm ahead or behind the fly, stayed on the spot for 2 seconds, moved backward or forward parallelly with the fly at 30 mm/s for a second, and then stayed on the spot for another 2 seconds before disappearing. (5 s)	1I-K, 2A-D, 5CD, S1B, S2F, S5EF
Translating objects on rotating backgrounds	A 10° x 10° black square appeared, stayed in place for a second, moved either back-to-front or front-to-back at 60 °/s for a second, and stayed for another second before disappearing. The midpoints of the trajectories were directly to the side of the fly. The background was either uniform mean gray or 5°-resolution, half-contrast random checkerboards that yaw-rotated around the fly at angular velocities ranging from -60 °/s to 60 °/s, with 20 °/s steps. (3 s)	1L-O, S1C
Azimuth sweep	A 10° x 10° black square swept 30° horizontal trajectories at 60°/s in either direction. The midpoints of the trajectories were positioned at 15°, 35°, 55°, 75°, 95°, or 115° to the side. (0.5 s)	1PQR, 2EF, S1D, S2J
Height sweep	A pair of mirror-symmetric objects with 10° width and various heights (5°, 10°, 20°, 40°, 80°) appeared and stayed in place for 2 seconds, moved either back-to-front or front-to-back at 60 °/s, then stayed in place for another 2 seconds before disappearing. The midpoints of the trajectories were directly to the sides of the fly. (5 s)	S3D-G
Rotational sinusoidal waves	Full-field, yaw-rotational, quarter-contrast drifting sinusoidal gratings with the spatial period of 60° and temporal frequency of 8 Hz. (0.5 s)	S2H
Translational sinusoidal waves	Same as the Rotational sinusoidal waves, but symmetrized about the fly such that it moved either back-to-front or front-to-back. (0.5 s)	S2G
Fast bars	A 10° wide and 106° tall bar appeared on the back of the fly and rotated around the fly at 60 °/s. (6 s)	S2I
Imaging experiments		
Stimulus	Description (duration)	Figures
Translating bars	A 10° wide bar extending the full vertical extent of the screen appeared at either -20° or +100° azimuth, and respectively moved at +60 °/s or -60 °/s for 2 seconds. (2 s)	3BC, 5G, S4I

Translating squares	A 10° x 10° square appeared at -20° elevation and either -20° or +100° azimuth, and respectively moved at +60 °/s or -60 °/s for 2 seconds. (2 s)	3BC, 5G, S4I
Expanding discs	A disc centered at +20° azimuth and -20° elevation linearly expanded with the initial and terminal radii of 0° and 60°. (2 s)	3B, 5G, S4I
Drifting square wave gratings	Full-contrast square wave gratings with the wavelength of 20° moved in the four cardinal directions at 60 °/s. (2 s)	3B, 4HI, 5G, S4I
Full-field flashes	The whole screen turned either uniform white or black. (2 s)	3B, 4HI, 5G, S4I
RF mapping stimulus	A 10° x 10° square moving in one of the four cardinal directions at 60 °/s, sweeping the 40° x 40° square area about the approximate receptive field center with 5° resolution. (0.67 s)	3DEF, S3BC
Height Sweep	A rectangular object with 10° width and various heights (5°, 10°, 20°, 40°, 60°, and the full vertical extent of the screen) moved horizontally in either direction at 60 °/s. (1 s)	3GH, 4LMN
Width Sweep	A rectangular object with 10° height and various widths (5°, 10°, 20°, 30°, 40°, 60°) moved horizontally in either direction at 60 °/s. (1 s)	3IJ
Velocity sweep	A 10° x 10° square moved horizontally at various velocities (10 °/s, 20 °/s, 30 °/s, 60 °/s, 120 °/s) in either direction, sweeping a 120° trajectory. (1 to 12 s)	S3HI
Flicker sweep	A 10° x 10° square appeared and flickered on the spot at various temporal frequencies (0.25 Hz, 1 Hz, 2 Hz, 4 Hz, 12 Hz, 20 Hz). (2 s)	S3JK
Translating objects on rotating backgrounds	A 10° x 10° black square appeared and moved horizontally in either direction at 60 °/s for 2 seconds on a background, which was either uniform gray or half-contrast, and consisted of 5° resolution checkerboards that yaw-rotated about the fly at velocities ranging from -60 °/s to +60 °/s with 20°/s steps. The background started a second prior to the onset of the square and lasted a second after the offset of the square. (4 s)	3KLM
Translating bars	A 10° wide bar extending the full vertical extent of the screen appeared at either -20° or +70° azimuth, and respectively moved at +60 °/s or -60 °/s for 1.5 seconds. (1.5 s)	4HI
Bars in four directions	A 10° wide vertical or horizontal bars respectively extending the full horizontal or vertical extent of the screen swept the whole screen at 60 °/s in the four cardinal directions. (4.5 s for vertical bars, 2 s for horizontal bars)	4KQR, S4D
Translating squares	A 10° x 10° square appeared at -30° elevation and either -20° or +100° azimuth, and respectively moved at +60 °/s or -60 °/s for 2 seconds. (2 s)	3NO, S3L
Translating rectangles (MI)	A 10° x 20° rectangle appeared at elevations around -20° chosen in every experiment and at either -20° or +100° azimuth, and respectively moved at +60 °/s or -60 °/s for 2 seconds. (2 s)	S3M

Translating rectangles (locomotion)	A 20° x 10° rectangle appeared at -20° elevation and either 0° or +120° azimuth, and respectively moved at +60 °/s or -60 °/s for 2 seconds. (2 s)	S3OP
Translating rectangles (RNAi)	A 20° x 10° rectangle appeared at -20° elevation and either -135° or +135° azimuth, and respectively moved at +60 °/s or -60 °/s for 4.5 seconds. (4.5 s)	4OP
Probe stimuli		
Stimulus	Description (duration)	Figures
Vertical bars	A 10° wide bar extending the full vertical extent of the screen appeared at either -20° or +70° azimuth, and respectively moved at +60 °/s or -60 °/s for 1.5 seconds. (1.5 s)	4HI
Bars in four directions	A 10° wide vertical or horizontal bars respectively extending the full horizontal or vertical extent of the screen swept the whole screen at 60 °/s in the four cardinal directions. (4.5 s for vertical bars, 2 s for horizontal bars)	4KQR, S4E
Translating squares	A 10° x 10° square appeared at -30° elevation and either -20° or +100° azimuth, and respectively moved at +60 °/s or -60 °/s for 2 seconds. (2 s)	3NO, S3L
Translating rectangles (MI)	A 10° x 20° rectangle appeared at elevations around -20° chosen in every experiment and at either -20° or +100° azimuth, and respectively moved at +60 °/s or -60 °/s for 2 seconds. (2 s)	S3M
Translating rectangles (locomotion)	A 20° x 10° rectangle appeared at -20° elevation and either 0° or +120° azimuth, and respectively moved at +60 °/s or -60 °/s for 2 seconds. (2 s)	S3OP
Translating rectangles (RNAi)	A 20° x 10° rectangle appeared at -20° elevation and either -135° or +135° azimuth, and respectively moved at +60 °/s or -60 °/s for 4.5 seconds. (4.5 s)	4OP

Table S2. Visual stimuli used in the study. Related to STAR Methods.

Supplemental References

S1. von Reyn, C.R., Nern, A., Williamson, W.R., Breads, P., Wu, M., Namiki, S., and Card, G.M. (2017). Feature Integration Drives Probabilistic Behavior in the Drosophila Escape Response. Neuron *94*, 1190-1204.e6.

S2. Morimoto, M.M., Nern, A., Zhao, A., Rogers, E.M., Wong, A.M., Isaacson, M.D., Bock, D.D., Rubin, G.M., and Reiser, M.B. (2020). Spatial readout of visual looming in the central brain of Drosophila. Elife *9*, e57685.

S3. Wu, M., Nern, A., Williamson, W.R., Morimoto, M.M., Reiser, M.B., Card, G.M., and Rubin, G.M. (2016). Visual projection neurons in the Drosophila lobula link feature detection to distinct behavioral programs. Elife *5*, e21022.

S4. Städele, C., Keleş, M.F., Mongeau, J.-M.M., and Frye, M.A. (2020). Non-canonical Receptive Field Properties and Neuromodulation of Feature-Detecting Neurons in Flies. Curr. Biol. *30*, 2508-2519.e6.

S5. Strother, J.A., Wu, S.-T., Rogers, E.M., Eliason, J.L.M., Wong, A.M., Nern, A., and Reiser, M.B. (2017). Behavioral state modulates the ON visual motion pathway of Drosophila. Proc. Natl. Acad. Sci. U. S. A., 201703090.

S6. Seelig, J.D., Chiappe, M.E., Lott, G.K., Dutta, A., Osborne, J.E., Reiser, M.B., and Jayaraman, V. (2010). Two-photon calcium imaging from head-fixed Drosophila during optomotor walking behavior. Nat. Methods *7*, 535–540.

S7. Fischbach, K.F., and Dittrich, A.P.M. (1989). The optic lobe of Drosophila melanogaster. I. A Golgi analysis of wild-type structure. Cell Tissue Res. *258*, 441–475.

S8. Scheffer, L.K., Xu, C.S., Januszewski, M., Lu, Z., Takemura, S.Y., Hayworth, K.J., Huang, G.B., Shinomiya, K., Maitin-Shepard, J., Berg, S., et al. (2020). A connectome and analysis of the adult drosophila central brain. Elife *9*, 1–74.